Enhancing teleportation via noisy channels: Effects of the induced multipartite entanglement

Víctor H. T. Brauer [*] and Andrea Valdés-Hernández [†]
Instituto de Física, Universidad Nacional Autónoma de México, Apartado Postal 20-364, Ciudad de México, Mexico

(Received 16 September 2023; accepted 12 April 2024; published 6 May 2024)

Quantum teleportation in the presence of noisy channels acting on a bipartite resource state is considered. We consider a family of generalized noisy channels that continuously connect the amplitude damping and the dephasing channels, encompassing a wide family of in-between scenarios, to delve into the relation between the teleportation success and the amount of three- and four-partite entanglement (distributed among the qubits of the resource state and those representing local environments) generated during the evolution. Our analysis reveals that for a fixed entanglement of the resource state, the channels that better protect the teleportation fidelity against the detrimental effects of noise are those that generate higher amounts of (Greenberger-Horne-Zeilinger–type) multipartite entanglement. This suggests that the dynamically induced multipartite correlations may serve as an additional resource for teleportation and provides insight into the characterization of processes and of the type of induced entanglement according to their ability to assist the protocol.

DOI: 10.1103/PhysRevA.109.052606

I. INTRODUCTION

Quantum teleportation stands out as one of the most fascinating applications of quantum entanglement. It allows the transmission of quantum information between two spatially separated agents, Alice and Bob, by means of local operations, classical communication, and a key element: a shared correlated state known as a resource state.[1] The original standard teleportation protocol [1] uses a (pure, maximally entangled, two-qubit) Bell state as the resource state. Subsequent investigations extended the scheme upon noticing that there exist resource states that are useful for teleportation yet are neither maximally entangled [2] nor pure, and their relation with violations of Bell inequalities [3,4] and discordlike correlations [5] has been discussed.

A mixed rather than a pure resource state is more realistic, particularly when taking into consideration the interaction of the (Alice and Bob) entangled pair with its surroundings, resulting in mixing of the resource state. There has been extensive research on such noisy quantum teleportation schemes [6–15], e.g., resorting to the Lindblad formalism to explore the fidelity of teleportation in terms of decoherence rates [6] or to determine the optimal Bell resource state under different local Pauli noises [7]. Recent methods for protecting teleportation against some decoherence channels have also been advanced [8,9]. The effect on the teleportation fidelity of different noisy channels acting on the resource state, typically representing the interaction of Alices's and Bob's particles with additional subsystems (which in the present case are regarded as local environments), has been studied considering the Kraus operators corresponding to dissipative interactions via an amplitude damping channel [10,11], together with other paradigmatic noise or decoherence channels on qubits such as bit flip, phase flip, depolarizing [12], and phase damping [13]. Also, the teleportation protocol under noisy channels in higher-dimensional systems has been explored [14]. A general theoretical and experimental [15] conclusion that ensues from these investigations is that there exist appropriate channels (acting on suitable initially pure resource states) for which the detrimental effects of noise on the teleportation fidelity are minimal compared to other noisy channels.

Further extensions of the original teleportation protocol have also been advanced that consider multiparty resource states exhibiting some type of multipartite entanglement. This has led to the development of strategies that exploit multipartite entanglement to teleport multiple qubit states as in, e.g., [16–20]. Multidirectional teleportation, allowing quantum information transmission between several agents, has also been explored [21–24], including the effect of noisy channels [25–28].

Despite the advances achieved regarding the teleportation success under noisy channels, whether acting on bipartite or multipartite resource states, the relation between the teleportation fidelity and the multipartite entanglement generated among the resource qubits and the environment has been much less explored. Such an analysis would allow us to identify the type of processes (characterized by the type of entanglement they induce) that favor a more successful teleportation and to possibly explain the fidelity improvement as an effect assisted by the created multipartite entanglement. In [29,30] some progress was made by relating the teleportation fidelity to the three-partite entanglement resulting from the local interaction of one qubit of the resource state with a two-level environment. Here we contribute along these lines,

[*] hernantorres@estudiantes.fisica.unam.mx
[†] andreavh@fisica.unam.mx

[1] Some authors refer to the resource state also as a quantum channel. Here we will keep the term quantum channel to denote a completely positive and trace-preserving map, which in the present context gives the reduced dynamics of an open system.

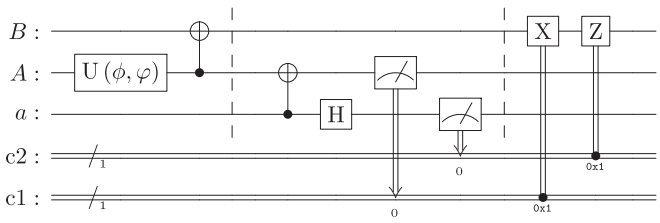

FIG. 1. Scheme of the standard teleportation protocol. Vertical dashed lines divide the different stages that correspond, from left to right, to (i) preparation of the initial resource state of the system $A + B$, (ii) application of a Bell measurement in Alice's qubits (a and A), and (iii) postprocessing according to Alice's results.

by focusing on the standard teleportation protocol in the presence of noisy channels acting on the bipartite resource state. We consider a generalized noisy quantum channel that can be continuously transformed from the amplitude damping to the dephasing channel [31] and explore the correlation between the maximal average fidelity and the amount of three- and four-partite entanglement, distributed among the pair of qubits that comprise the resource state and the qubits that represent the corresponding local environments.

We first revisit the standard teleportation protocol and the notion of maximal average fidelity $F_{\max}$ as a quantifier of the teleportation success (Sec. II) and express the latter in terms of the Kraus operators of an arbitrary quantum channel acting on the (arbitrary yet initially pure) resource state, comprised of two qubits A and B (Sec. III). After these preliminary sections, we relate the maximal average fidelity above the classical threshold value, $\mathbb{F}_{\max}$, to the bipartite entanglement between A and B, considering $A + B$ as an ideal closed system (Sec. IV). Assuming then that B interacts with a local two-level environment E_B via the generalized channel, we investigate the relation between $\mathbb{F}_{\max}$ and the three-partite entanglement distributed among A, B, and E_B (Sec. V). The analysis is extended to the four-partite case by considering that both A and B locally interact with their respective environments E_A and E_B under independent generalized channels, and a nontrivial correlation between $\mathbb{F}_{\max}$ and the four-partite entanglement is disclosed (Sec. VI). Finally, a summary and some concluding remarks are presented (Sec. VII).

II. STANDARD TELEPORTATION PROTOCOL AND MAXIMAL AVERAGE FIDELITY

The main idea behind the standard teleportation protocol is that Alice wants to send to Bob an arbitrary input state ρ_{in} encoded in a qubit a in her possession. For this task, they share a pair of qubits A and B (in Alice's and Bob's possession, respectively) in an entangled state ρ_{AB}, called resource state. Alice then performs a Bell measurement [32–34] on her pair of qubits a and A and communicates the outcome to Bob via a classical channel. Upon receiving this information, and knowing ρ_{AB} [35], Bob performs a unitary operation $\sigma^{(i)} \in \{\mathsf{I}_2, \sigma^x, \sigma^y, \sigma^z\}$ on his qubit B, thus putting it into the output state ρ_{out} ($\sigma^{x,y,z}$ stand for the Pauli matrices and I_n denotes the $n \times n$ identity operator). Figure 1 shows a schematic generalization of the standard teleportation protocol. The qubits A and B are initially in the state $|0\rangle$, whereas a is already in ρ_{in}, the state to be teleported. Vertical dashed lines separate the different stages of the protocol corresponding, from left to right, to the following.

(i) A unitary transformation $U(\phi, \varphi)$ rotates the qubit A and a controlled-NOT (CNOT) gate is employed to prepare the initial resource state

$$|\phi_0\rangle_{AB} = \cos\phi|00\rangle + e^{i\varphi}\sin\phi|11\rangle, \tag{1}$$

with $\phi \in [0, \pi/2]$ and $\varphi \in [-\pi/2, 3\pi/2]$. [This generalizes the application of the Hadamard gate, resulting in the Bell state $\frac{1}{\sqrt{2}}(|00\rangle + |11\rangle)$.]

(ii) Alice applies a CNOT and a Hadamard gate to the qubits in her possession and then performs a measurement in the Bell basis and communicates the outcome to Bob via classical channels.

(iii) Depending on Alice's measurement outcome, Bob applies appropriate unitary operations on his qubit B, so the output state of B coincides with the input state of a. The whole strategy leads to perfect teleportation if the resource state (1) is the Bell state $\frac{1}{\sqrt{2}}(|00\rangle + |11\rangle)$ (if $|\phi_0\rangle$ is another Bell state, then the operations in Bob's strategy must be changed).

For pure input states $\rho_{\text{in}} = |\chi\rangle\langle\chi|$, the success of the teleportation can be quantified by means of the maximal average fidelity $F_{\max}$, which measures the probability that ρ_{out} coincides with the (unknown) ρ_{in}, averaged over all input states, provided the appropriate $\sigma^{(i)}$ is chosen. The maximal average fidelity for an arbitrary two-qubit resource state ρ_{AB} can be written as [36]

$$F_{\max} = \tfrac{1}{3}[2\mathcal{F}_{\max}(\rho_{AB}) + 1], \tag{2}$$

where $\mathcal{F}_{\max}$ is the maximal singlet fraction [37]

$$\mathcal{F}_{\max} = \max_i\{\langle\Phi_i|\rho_{AB}|\Phi_i\rangle\} \tag{3}$$

corresponding to the maximum fidelity between the resource state and any of the Bell states[2]

$$|\Phi_i\rangle = (\mathsf{I}_2 \otimes \sigma^{(i)})|\Phi^+\rangle, \quad |\Phi^+\rangle = \frac{1}{\sqrt{2}}(|00\rangle + |11\rangle). \tag{4}$$

Setting $\sigma^{(0)} = \mathsf{I}_2$ and $\sigma^{(1),(2),(3)} = \sigma^{x,y,z}$, we get

$$|\Phi_{0/3}\rangle = |\Phi^\pm\rangle = \frac{1}{\sqrt{2}}(|00\rangle \pm |11\rangle),$$
$$|\Phi_{1/2}\rangle = |\Psi^\pm\rangle = \frac{1}{\sqrt{2}}(|01\rangle \pm |10\rangle). \tag{5}$$

Therefore, $\mathcal{F}_{\max}$ picks out the optimal Bell state, i.e., the Bell state that is closest to ρ_{AB}. The above expressions show that if ρ_{AB} is a Bell state, the protocol guarantees the complete reconstruction of the input state.

For the quantum teleportation to be considered successful $F_{\max}$ must be greater than $\frac{2}{3}$, which is the value of the maximal

[2]In Ref. [37] the maximal singlet fraction was defined considering the maximum over all the maximally entangled states. Here we maximize only over those states that can be obtained from Bell states by means of unitary transformations of the form $\mathsf{I}_2 \otimes \sigma^{(i)}$. With this restriction we adhere to the standard teleportation protocol (in which Bob's operations are implemented via Pauli operators).

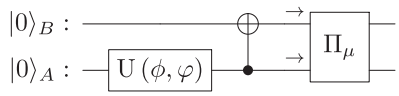

FIG. 2. The pair of qubits A and B, once in the entangled state $|\phi_0\rangle$, passes through an arbitrary quantum channel represented by the set of Kraus operators Π_μ, resulting in a mixed resource state ρ_{AB}.

average fidelity corresponding to the best possible reconstruction through a purely classical channel [38]. Throughout this paper we will be interested in the success of nonclassical teleportation; hence we will focus on those regimes in which $F_{\max} \geqslant \frac{2}{3}$ and accordingly pay attention to the quantity

$$\mathbb{F}_{\max} = \max\left\{\tfrac{2}{3}, F_{\max}\right\}. \tag{6}$$

III. MAXIMAL AVERAGE FIDELITY UNDER QUANTUM CHANNELS

Let us assume that A and B are initially prepared in the state $|\phi_0\rangle_{AB}$, given by Eq. (1), which then passes through a quantum channel Λ_{AB} represented by a set of Kraus operators $\{\Pi_\mu\}$, acting on $\mathcal{H}_A \otimes \mathcal{H}_B$ [39]. A scheme of this process is shown in Fig. 2. The channel thus transforms $|\phi_0\rangle\langle\phi_0|$ into an effective (typically mixed) resource state ρ_{AB} given by

$$\rho_{AB} = \Lambda_{AB}(|\phi_0\rangle\langle\phi_0|) = \sum_\mu \Pi_\mu |\phi_0\rangle\langle\phi_0|\Pi_\mu^\dagger. \tag{7}$$

Direct substitution into Eq. (3) gives, with the aid of (2),

$$F_{\max} = \frac{1}{3} + \frac{2}{3}\max_i \left\{\sum_\mu |\langle\Phi_i|\Pi_\mu|\phi_0\rangle|^2\right\}. \tag{8}$$

This simple but central expression for $F_{\max}$ in terms of the Kraus operators allows for studying the teleportation success when the initially pure resource state is subject to an arbitrary quantum channel.

Since Alice and Bob are typically spatially separated, we will focus on cases in which A and B undergo independent local channels, so $\Lambda_{AB} = \Lambda_A \otimes \Lambda_B$ and

$$\Pi_\mu \to \Pi_{\alpha\beta} = Q_\alpha \otimes K_\beta, \tag{9}$$

where $\{Q_\alpha\}$ and $\{K_\beta\}$ stand for the sets of Kraus operators associated with Λ_A and Λ_B, respectively, each set having at most $(\dim \mathcal{H}_{A\,(B)})^2 = 4$ elements. Equation (8) becomes then

$$F_{\max} = \frac{1}{3} + \frac{2}{3}\max_i \left\{\sum_{\alpha\beta} |\langle\Phi_i|Q_\alpha \otimes K_\beta|\phi_0\rangle|^2\right\}. \tag{10}$$

The channel $\Lambda_A \otimes \Lambda_B$ acts as if A and B interact locally with a corresponding party E_A and E_B. Assuming that the systems $A + B$, E_A, and E_B are initially uncorrelated and that E_A and E_B are qubits in the initial state $|0\rangle$, we may write

$$|\psi_0\rangle_{ABE_AE_B} = |\phi_0\rangle_{AB} \otimes |0\rangle_{E_A} \otimes |0\rangle_{E_B} \tag{11}$$

for the initial four-partite state. Further, if the interaction between A and E_A is represented by the unitary operator U_{AE_A} (and similarly for B and E_B), then

$$Q_\alpha = {}_{E_A}\langle\alpha|U_{AE_A}|0\rangle_{E_A}, K_\beta = {}_{E_B}\langle\beta|U_{BE_B}|0\rangle_{E_B}, \tag{12}$$

with $\{|\alpha\rangle\}$ and $\{|\beta\rangle\}$ bases of $\mathcal{H}_{E_A}$ and $\mathcal{H}_{E_B}$, respectively. In addition, the (unitary) evolution of the complete system can be obtained from these Kraus operators as

$$\begin{aligned}|\psi\rangle_{ABE_AE_B} &= U_{AE_A}U_{BE_B}|\psi_0\rangle_{ABE_AE_B} \\ &= \sum_{\alpha\beta} Q_\alpha K_\beta |\phi_0\rangle_{AB}|\alpha\rangle_{E_A}|\beta\rangle_{E_B}.\end{aligned} \tag{13}$$

A particular family of local channels, which involves a three-party system instead of a four-partite one, is that in which one of the resource qubits, say, A, remains unaffected so $\Lambda_A = \mathrm{I}_2$, while B goes through an arbitrary channel Λ_B. In this case $Q_\alpha = \mathrm{I}_2\delta_{\alpha 0}$, and from Eq. (10) we are led to

$$F_{\max} = \frac{1}{3} + \frac{2}{3}\max_i \left\{\sum_\beta |\langle\Phi_i|(\mathrm{I}_2 \otimes K_\beta)|\phi_0\rangle|^2\right\}. \tag{14}$$

Clearly for $\Lambda_{AB} = \mathrm{I}_2 \otimes \Lambda_B$ the subsystem E_A is superfluous, and Eq. (11) reduces to the three-qubit initial state

$$|\psi_0\rangle_{ABE_B} = |\phi_0\rangle_{AB} \otimes |0\rangle_{E_B}. \tag{15}$$

IV. FIDELITY AND BIPARTITE ENTANGLEMENT IN THE STANDARD TELEPORTATION PROTOCOL

The standard protocol, depicted in the circuit of Fig. 1, corresponds to $\Lambda_{AB} = \mathrm{I}_4$. Equation (8) thus becomes

$$F_{\max} = \tfrac{1}{3} + \tfrac{2}{3}\max_i\{|\langle\Phi_i|\phi_0\rangle|^2\}. \tag{16}$$

With $|\phi_0\rangle$ given by (1), the optimal strategy corresponds to the state $|\Phi^+\rangle$ for $\varphi \in [-\frac{\pi}{2}, \frac{\pi}{2}]$ and $|\Phi^-\rangle$ for $\varphi \in [\frac{\pi}{2}, \frac{3\pi}{2}]$, so (16) reduces to $F_{\max} = \frac{2}{3} + \frac{1}{3}\mathcal{E}_0|\cos\varphi|$ and consequently, in the noninteracting case, Eq. (6) gives

$$\mathbb{F}_{\max}^{\text{nonint}} = \tfrac{2}{3} + \tfrac{1}{3}\mathcal{E}_0|\cos\varphi|, \tag{17}$$

where $\mathcal{E}_0$ stands for the entanglement of the initial resource state

$$\mathcal{E}_0 \equiv C(|\phi_0\rangle) = 2\cos\phi\sin\phi = \sin 2\phi. \tag{18}$$

Here C is the concurrence, quantifying the amount of qubit-qubit entanglement [40]. For an arbitrary (in general mixed) two-qubit state ρ_{AB} it is defined as

$$C_{AB} \equiv C(\rho_{AB}) = \max\{0, \sqrt{\lambda_0} - \sqrt{\lambda_1} - \sqrt{\lambda_2} - \sqrt{\lambda_3}\}, \tag{19}$$

where $\{\lambda_n\}$ are the eigenvalues of the matrix $\rho_{AB}(\sigma^y \otimes \sigma^y)\rho_{AB}^*(\sigma^y \otimes \sigma^y)$ ordered in decreasing order and ρ_{AB}^* stands for the complex conjugate of ρ_{AB} expressed in the computational basis. When the state is pure ($\rho_{AB} = |\chi\rangle\langle\chi|$), the expression for the concurrence simplifies and reads

$$C_{AB} = C(|\chi\rangle) = \sqrt{2\big(1 - \mathrm{Tr}\rho_A^2\big)} = \sqrt{2\big(1 - \mathrm{Tr}\rho_B^2\big)}, \tag{20}$$

with $\rho_{A\,(B)} = \mathrm{Tr}_{B\,(A)}\rho_{AB}$ the reduced density matrix of either one of the qubits.

Equation (17) makes explicit that the teleportation success is enhanced as the resource state's entanglement $\mathcal{E}_0$ increases. It also shows that as φ tends to $\pm\pi/2$, the fidelity decreases up to its minimal (classically attainable) value $\frac{2}{3}$, irrespective of the initial entanglement, as can be seen in Fig. 3. In other words, there are maximally entangled resource states for which the maximal average fidelity does not exceed its

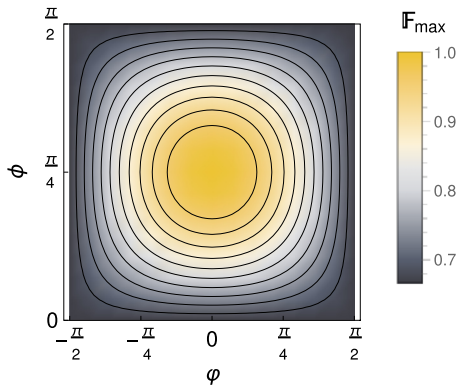

FIG. 3. Maximal average fidelity in the absence of interaction [Eq. (17)] as a function of φ and ϕ, in color scale ranging from $\frac{2}{3}$ to 1. At $\varphi = \pm\pi/2$, $\mathbb{F}_{\max}^{\text{nonint}}$ shows no improvement with respect to the classically attainable value ($\frac{2}{3}$), irrespective of ϕ, which determines the initial entanglement $\mathcal{E}_0 = \sin 2\phi$.

classical limit, and the relative phase φ determines the fraction of $\mathcal{E}_0$ that ultimately improves the fidelity.

V. FIDELITY AND THREE-PARTITE ENTANGLEMENT GENERATED VIA A NOISY CHANNEL

We now focus on the case in which only B goes through a quantum channel, effectively representing an interaction with an additional qubit E_B. Figure 4 illustrates this situation, leading to a mixed resource state ρ_{AB} before the measurement stage of the protocol.

The scenario under consideration corresponds to that in which $|\phi_0\rangle\langle\phi_0|$ is subject to a channel $\Lambda_{AB} = \mathrm{I}_2 \otimes \Lambda_B$, where Λ_B encodes the interaction between B and E_B, giving rise to the possible creation of tripartite entanglement in the system $A + B + E_B$. The channel thus transforms the initial state (15)

$$|\psi_0\rangle_{ABE_B} = \cos\phi|000\rangle + e^{i\varphi}\sin\phi|110\rangle \tag{21}$$

into the three-qubit state [see Eq. (13) with $Q_\alpha = \mathrm{I}_2\delta_{\alpha 0}$]

$$|\psi\rangle_{ABE_B} = \sum_\beta K_\beta|\phi_0\rangle_{AB}|\beta\rangle_{E_B}. \tag{22}$$

In [41] necessary and sufficient conditions on the Kraus operators $K_\beta = \langle\beta|U_{BE_B}|0\rangle$ were established that ensure the emergence of bipartite and tripartite entanglement among the parties A, B, and E_B. For the present analysis we concentrate on the dynamics of the resource state's (bipartite) entanglement $C_{AB} = C(\rho_{AB})$ and the tripartite entanglement, as measured by the so-called 3-tangle. The latter stands as

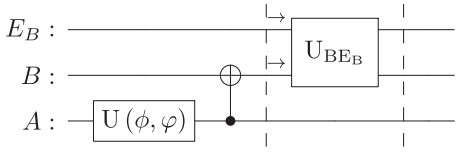

FIG. 4. Qubits A, B, and E_B are prepared in the initial state (15). Then B and E_B interact via a unitary operation U_{BE_B}, and the effect on B is that of a quantum channel described by the Kraus operators $\{K_\beta\}$.

a legitimate measure of residual entanglement in a three-qubit pure state $|\psi\rangle_{ijk}$ and quantifies the amount of three-way Greenberger-Horne-Zeilinger (GHZ)–type entanglement in the state [42]. The 3-tangle is defined as [43]

$$\tau_{ijk} = \tau(|\psi\rangle_{ijk}) = C_{i|jk}^2 - C_{ij}^2 - C_{ik}^2, \tag{23}$$

where C_{ij} is given by Eq. (19) and $C_{i|jk}$ by

$$C_{i|jk} = \sqrt{2\left(1 - \mathrm{Tr}\rho_i^2\right)}. \tag{24}$$

This expression generalizes (20) for a three-party pure state and quantifies the entanglement across the bipartition $i|(j+k)$ [44].

In [41] it was found that for $\Lambda_{AB} = \mathrm{I}_2 \otimes \Lambda_B$, C_{AB} and τ_{ABE_B} evolve according to

$$C_{AB}^2 = \mathcal{E}_0^2(|\det K_0| + |\det K_1|)^2 - \tfrac{1}{2}\mathcal{E}_0^2(|u| - |v| + |v - u|) \tag{25}$$

and

$$\tau_{ABE_B} = \mathcal{E}_0^2|u - v|, \tag{26}$$

where $u = 4\det K_0 K_1$ and $v = g^2(K_0, K_1)$, with $g(M,N) = \mathrm{Tr}M\,\mathrm{Tr}N - \mathrm{Tr}(MN)$. The evolution parameter is encoded in the Kraus operators and is not explicitly written in the above expressions.

A. Generalized noisy channel

In order to study the role of the 3-tangle in the teleportation fidelity, we focus on channels Λ_B whose Kraus operators have the structure [31] [in the basis $\{|0\rangle = (1,0)^\top, |1\rangle = (0,1)^\top\}$ of $\mathcal{H}_B$]

$$K_0 = \begin{pmatrix} 1 & 0 \\ 0 & \sqrt{1-p} \end{pmatrix}, \quad K_1 = \sqrt{p}\begin{pmatrix} 0 & \cos\zeta \\ 0 & \sin\zeta \end{pmatrix}, \tag{27}$$

where $\zeta \in [0, \pi/2]$ and $0 \leqslant p \leqslant 1$. From the second of Eqs. (12) and the explicit form of K_0 in (27), we get $\langle 1|K_0|1\rangle = \langle 10|U_{BE_B}|10\rangle = \sqrt{1-p}$. This means that under U_{BE_B}, the state $|10\rangle$ transforms into a state that is written as

$$U_{BE_B}|10\rangle = \sqrt{1-p}|10\rangle + \sqrt{p}e^{i\theta}|10_\perp\rangle, \tag{28}$$

with $|10_\perp\rangle$ a normalized state that is orthogonal to $|10\rangle$. Consequently, p can be interpreted as the probability that the state $|10\rangle_{BE_B}$ evolves into an orthogonal state under the transformation U_{BE_B}. Clearly p is a function of the evolution parameter of U_{BE_B}, typically the time for Hamiltonian evolutions $U_{BE_B}(t) = e^{-iHt/\hbar}$. For $U_{BE_B}(0) = \mathrm{I}_4$, p initially vanishes and then increases up to $p = 1$ when the state $|10_\perp\rangle$ (completely distinguishable from $|10\rangle$) is reached. This allows us to identify p as a useful parameter to track the evolution induced by U_{BE_B}, without making specific assumptions regarding such a unitary transformation.

Each value of the parameter ζ in (27) determines a specific channel, so a comparison of the dynamics under different channels can be achieved by varying the values of ζ. When $\zeta = 0$, Eqs. (27) reduce to the Kraus operators of the amplitude damping channel (AC), whereas for $\zeta = \pi/2$ the Kraus operators of the dephasing channel (DC) are recovered. The AC and the DC are paradigmatic decoherence channels [45]

that generate W-type and GHZ-type genuine entanglement, respectively, in the three-qubit system [41,46,47]. By means of Eqs. (27), corresponding to what we will call the generalized (noisy) channel (GC), we can analyze intermediate situations lying between the AC and the DC and particularly extend some of the results reported in, e.g., [15,29,30], to a wider range of channels.

When B is subject to the GC, the evolved state (22) reads explicitly

$$|\psi\rangle = \cos\phi|000\rangle + e^{i\varphi}\sin\phi(\sqrt{1-p}|110\rangle + \sqrt{p}\cos\zeta|101\rangle + \sqrt{p}\sin\zeta|111\rangle). \tag{29}$$

The entanglement of the corresponding resource state and the generated amount of 3-tangle become, using Eqs. (25) and (26),

$$C_{AB} = \mathcal{E}_0\sqrt{1-p}, \quad \tau_{ABE_B} = \mathcal{E}_0^2 p\sin^2\zeta, \tag{30}$$

so only the 3-tangle depends on the specific channel. Further, $p\sin^2\zeta$ determines the fraction of the initial entanglement $\mathcal{E}_0$ that can be converted into three-partite entanglement. For fixed $\mathcal{E}_0$ and p, as ζ increases from 0 to $\pi/2$ the 3-tangle goes from its minimum (0) to its maximum ($\mathcal{E}_0^2 p$) value. The minimum corresponds to the AC case ($\zeta = 0$) and the maximum to the DC case ($\zeta = \pi/2$), which is the only channel for which all the initial entanglement can be transformed into the 3-tangle (at $p = 1$).

From Eq. (14) it follows that for B subject to the GC, the maximal average fidelity can be written as $F_{\max} = \max_i\{F_{\Phi_i}\}$, with

$$F_{\Phi_i} = \frac{1}{3} + \frac{2}{3}\sum_\beta |\langle\Phi_i|(\mathrm{I}_2 \otimes K_\beta)|\phi_0\rangle|^2. \tag{31}$$

Direct calculation gives

$$F_{\Phi^\pm} = \tfrac{2}{3} + \tfrac{1}{3}(\pm\mathcal{E}_0\sqrt{1-p}\cos\varphi - \mathcal{P}_1 p\cos^2\zeta), \tag{32a}$$

$$F_{\Psi^+} = F_{\Psi^-} = \tfrac{2}{3} - \tfrac{1}{3}(1 - \mathcal{P}_1 p\cos^2\zeta), \tag{32b}$$

where

$$\mathcal{P}_1 = \sin^2\phi \tag{33}$$

stands for the initial population of the state $|11\rangle_{AB}$. On one hand, $\mathcal{P}_1 p\cos^2\zeta \leqslant 1$ implies that $F_{\Psi^\pm} \leqslant \frac{2}{3}$. On the other hand,

$$\max\{F_{\Phi^+}, F_{\Phi^-}\} = \begin{cases} F_{\Phi^+}, & \varphi \in [-\pi/2, \pi/2] \\ F_{\Phi^-}, & \varphi \in [\pi/2, 3\pi/2] \end{cases} = \frac{2}{3} + \frac{1}{3}(\mathcal{E}_0\sqrt{1-p}|\cos\varphi| - \mathcal{P}_1 p\cos^2\zeta). \tag{34}$$

Consequently, under the generalized channel, the quantity of interest (6) is given by

$$\mathbb{F}_{\max}^{\mathrm{GC}} = \tfrac{2}{3} + \tfrac{1}{3}\max\{0, [C_{AB}(p)|\cos\varphi| - \mathcal{P}_1 p\cos^2\zeta]\}, \tag{35}$$

where we have used Eq. (30) for C_{AB}. It follows from Eq. (35) that, as in the noiseless scenario [see Eq. (17)], when the maximal average fidelity exceeds the classical threshold it has a non-negative contribution proportional to the entanglement of the resource state, attenuated by $|\cos\varphi|$. This indicates that, as in the noiseless case, the optimal φ is $0, \pi$. In the GC case, however, an additional negative contribution (a loss in the fidelity) appears that depends on the channel (via $\cos^2\zeta$), the evolution p, and the initial excited population $\mathcal{P}_1$. For fixed $\mathcal{P}_1$ and p, such loss decreases as $\tau_{ABE_B} \sim \sin^2\zeta$ increases. This means that given an initial state, at each stage of the evolution (determined by a fixed p), the channels that produce higher amounts of 3-tangle lead to higher values of the maximum average fidelity.

TABLE I. Values of C_{AB}, $\mathbb{F}_{\max}^{\mathrm{GC}}$, and τ_{ABE_B} taken from Fig. 5 (corresponding to $\phi = \pi/4$ and $\varphi = 0$) for $p = 0.8$ and different values of the channel parameter ζ.

ζ	C_{AB}	$\mathbb{F}_{\max}^{\mathrm{GC}}$	τ_{ABE_B}
0	0.447214	0.682405	0
$\pi/6$	0.447214	0.715738	0.2
$\pi/4$	0.447214	0.749071	0.4
$\pi/3$	0.447214	0.782405	0.6
$\pi/2$	0.447214	0.815738	0.8

The above conclusion can also be extracted from Fig. 5, which shows C_{AB}, $\mathbb{F}_{\max}^{\mathrm{GC}}$, and τ_{ABE_B} for different values of ζ and varying p, considering a maximally entangled initial state ($\phi = \pi/4$) and setting φ to its optimal value $\varphi = 0$. At $p = 0$, $\mathbb{F}_{\max}^{\mathrm{GC}}$ reduces to $\mathbb{F}_{\max}^{\mathrm{nonint}}$, no 3-tangle exists, and the success of the teleportation is ascribable to the (bipartite) entanglement $\mathcal{E}_0 = C_{AB}(0)$ only, in line with the discussion in Sec. IV. As p increases, the action of Λ_B degrades the entanglement of the resource state (whose dynamics is independent of ζ) and a concomitant gradual loss in the maximal average fidelity is observed for all ζ. This is an expected behavior under generic local channels $\Lambda_A \otimes \Lambda_B$ (meaning nonincreasing entanglement operations).

In its turn, as p increases the 3-tangle increases as well, as a result of the redistribution of the entanglement. Therefore, for any given generalized noisy channel, the decay of the maximal average fidelity along the evolution is accompanied by an increase of the 3-tangle. The question then arises as to under which channels $\mathbb{F}_{\max}^{\mathrm{GC}}$ is more robust against the noise, that is, under which channels the loss in the teleportation success is reduced at any stage of the evolution. To answer it, we compare the values of $\mathbb{F}_{\max}^{\mathrm{GC}}$ for all possible GCs while keeping p fixed. A comparison of Figs. 5(b) and 5(c) shows that the decaying path of $\mathbb{F}_{\max}^{\mathrm{GC}}$ varies with ζ in such a way that for each and every p, the channels that generate higher amounts of 3-tangle yield higher fidelities. Table I exemplifies this by explicitly showing the values of $\mathbb{F}_{\max}^{\mathrm{GC}}$ and τ_{ABE_B} extracted from Fig. 5 for $p = 0.8$. While the entanglement of the resource state is constant as ζ varies [see the first of Eqs. (30)], the maximal average fidelity and the 3-tangle change in a correlated fashion: An increase in τ_{ABE_B} is accompanied by an increase in $\mathbb{F}_{\max}^{\mathrm{GC}}$. This behavior is replicated for any other value of $p \in (0, 1)$.

Therefore, despite the adverse influence of noise on the fidelity, the detrimental effects are lessened under channels that give rise to higher amounts of tripartite entanglement. It is in this sense that the 3-tangle improves the teleportation success and may help to maintain $\mathbb{F}_{\max}^{\mathrm{GC}}$ above the classical

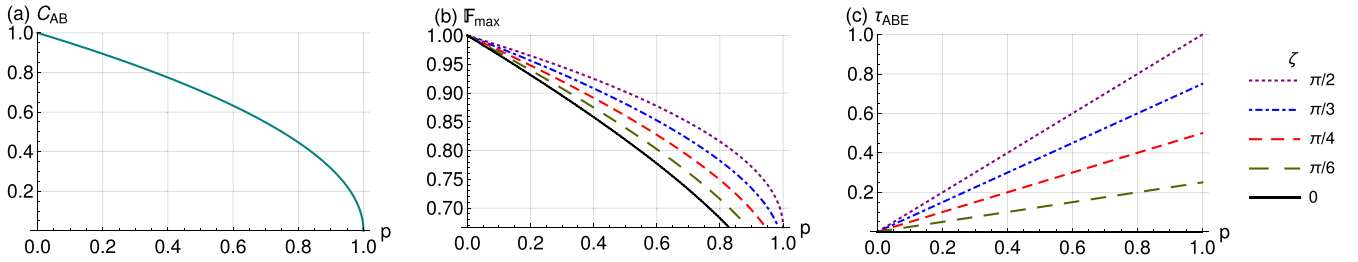

FIG. 5. Evolution of (a) the entanglement of the resource state, (b) the maximal average fidelity above the classical threshold value, and (c) the 3-tangle when the qubit B is subject to a GC, for different values of the channel parameter $\zeta \in [0, \pi/2]$, $\phi = \pi/4$, and $\varphi = 0$. The channel induces a loss in the resource entanglement C_{AB}, and the teleportation fidelity decreases accordingly. However, when different channels (values of ζ) are considered, it is observed that those that generate more 3-tangle favor higher fidelities at each p. Therefore, as ζ increases from 0 (amplitude damping channel) to $\pi/2$ (dephasing channel), the generated 3-tangle helps to enhance the maximal average fidelity (provided $C_{AB} \neq 0$).

threshold value longer, i.e., for larger values of p, as seen in Fig. 5(b).

It is also clear from Fig. 5 that the channel that gives better fidelities throughout the evolution is the DC, corresponding to $\zeta = \pi/2$. Only for this channel, $\mathbb{F}_{\max}^{\mathrm{GC}}$ exceeds the classically attainable value for all $0 < p < 1$. This holds not only for a maximally entangled initial state, but also for $\mathcal{E}_0 \neq 0$. In fact, it follows from Eq. (35) that the condition $\mathbb{F}_{\max}^{\mathrm{GC}} > \frac{2}{3}$ amounts to

$$\mathcal{P}_1 p \cos^2\zeta < C_{AB}(p)|\cos\varphi| = \mathcal{E}_0\sqrt{1-p}|\cos\varphi|, \tag{36}$$

which is trivially satisfied for $p \in (0, 1)$ and $\mathcal{E}_0 \neq 0$ taking $\zeta = \pi/2$. Further, by writing $\mathcal{E}_0 = 2\sqrt{\mathcal{P}_1(1-\mathcal{P}_1)}$, the condition (36) is rewritten as

$$\frac{1}{2}\frac{\cos^2\zeta}{|\cos\varphi|}\frac{p}{\sqrt{1-p}} < \sqrt{\frac{1-\mathcal{P}_1}{\mathcal{P}_1}}, \tag{37}$$

which exhibits the role of the initial population $\mathcal{P}_1$ in the dynamics of $\mathbb{F}_{\max}^{\mathrm{GC}}$ (assuming fixed φ and ζ): The left-hand side of the inequality is an increasing function of p, whereas the upper bound decreases with $\mathcal{P}_1$; consequently, as $\mathcal{P}_1$ increases the inequality becomes more restrictive and a point in the evolution is reached sooner (for lower values of p) at which (37) no longer holds and the fidelity drops below the threshold value $\frac{2}{3}$.

Finally, as $p \to 1$ we have $C_{AB} \to 0$, and from Eq. (35) $\mathbb{F}_{\max}^{\mathrm{GC}}$ cannot exceed $\frac{2}{3}$ despite τ_{ABE_B} attaining its maximum value. This evinces that even though the presence of tripartite entanglement improves the teleportation success (in the sense described above), a nonzero entanglement of the resource state is key to triggering the potential of the 3-tangle to assist the teleportation.

Figure 6 shows, at different stages of the evolution, curves in the space $(\tau_{ABE_B}, \mathbb{F}_{\max}^{\mathrm{GC}})$ sweeping as the channel parameter goes from $\zeta = 0$ (AC, black circles) to $\zeta = \pi/2$ (DC, red stars). Each trajectory corresponds to an initial state determined by $\phi = \pi/6$ (red dashed line), $\phi = \pi/4$ (black solid line), and $\phi = \pi/3$ (blue dash-dotted line), all with $\varphi = 0$. In all curves the relation between the 3-tangle and the maximal average fidelity discussed above is manifest: Throughout the evolution, better fidelities are attained under channels that produce higher amounts of 3-tangle.

Interestingly, Fig. 6 shows that whereas an initial resource state with maximal entanglement ($\phi = \pi/4$) leads to the highest value of $\mathbb{F}_{\max}^{\mathrm{GC}}$ (for sufficiently large values of τ_{ABE_B}), a maximally entangled state is not always the optimal one for achieving a better fidelity. This is clearly seen, for example, in Fig. 6(c), where the fidelity for $\phi = \pi/6$ ($\mathcal{E}_0 \sim 0.866$) is greater than that corresponding to $\phi = \pi/4$ ($\mathcal{E}_0 = 1$) for some channels. Moreover, noticing that $\phi = \pi/3$ gives the same $\mathcal{E}_0$ as $\phi = \pi/6$, the difference between the red dashed and blue dash-dotted curves reveals the effect of the initial population $\mathcal{P}_1$ on the behavior of $\mathbb{F}_{\max}^{\mathrm{GC}}$. In particular, for $\phi = \pi/3$ we have $\mathcal{P}_1 = 0.75$, while for $\phi = \pi/6$ we have $\mathcal{P}_1 = 0.25$. As seen from Eq. (35), the greater the $\mathcal{P}_1$, the greater the loss in the fidelity (which goes as $-\mathcal{P}_1 p\cos^2\zeta$), which explains why the blue dash-dotted line runs below the red dashed one, despite both curves corresponding to the same initial entanglement.

In summary, from all the generalized channels acting on B, those that improve the quantum teleportation success (at each instant) are the ones that produce higher amounts of 3-tangle among the qubits A, B, and E_B. The optimal channel corresponds to $\zeta = \pi/2$ (DC) and the worst to $\zeta = 0$ (AC). This can be seen graphically and is corroborated by Eq. (35), which gives

$$\mathbb{F}_{\max}^{\mathrm{AC}} \leqslant \mathbb{F}_{\max}^{\mathrm{GC}} \leqslant \mathbb{F}_{\max}^{\mathrm{DC}}, \tag{38}$$

with

$$\mathbb{F}_{\max}^{\mathrm{DC}} = \tfrac{2}{3} + \tfrac{1}{3}C_{AB}(p)|\cos\varphi| \tag{39}$$

and

$$\begin{aligned}\mathbb{F}_{\max}^{\mathrm{AC}} &= \tfrac{2}{3} + \tfrac{1}{3}\max\{0, C_{AB}(p)|\cos\varphi| - \mathcal{P}_1 p\} \\ &= \max\left\{\tfrac{2}{3}, \mathbb{F}_{\max}^{\mathrm{DC}} - \tfrac{1}{3}\mathcal{P}_1 p\right\}.\end{aligned} \tag{40}$$

Below we explore in more detail the states produced by the limiting cases of the DC and AC.

B. Amplitude damping channel vs dephasing channel

The DC produces GHZ-type states, whose form follows from Eq. (29) with $\zeta = \pi/2$:

$$\begin{aligned}|\psi_{\mathrm{GHZ}}\rangle &\equiv |\psi(\zeta = \pi/2)\rangle \\ &= \cos\phi|000\rangle + e^{i\varphi}\sin\phi(\sqrt{1-p}|110\rangle \\ &\quad + \sqrt{p}|111\rangle).\end{aligned} \tag{41}$$

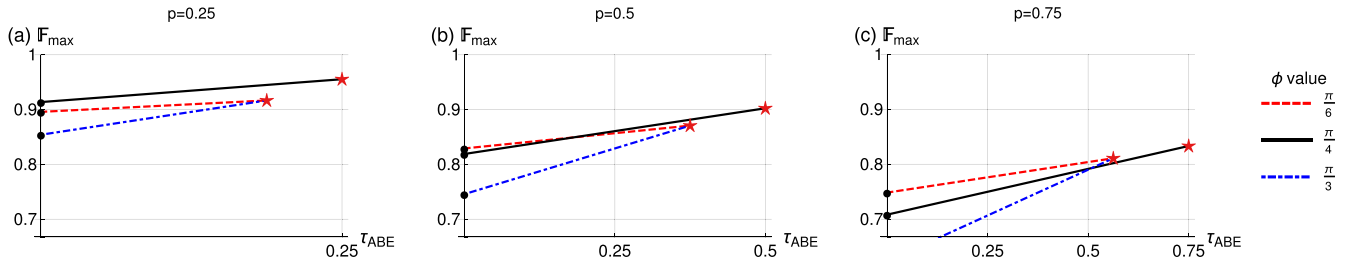

FIG. 6. Trajectories in the space $(\tau_{ABE_B}, \mathbb{F}_{\max}^{GC})$ as the channel parameter ζ runs from 0 (black circles) to $\pi/2$ (red stars), for three initial states with $\phi = \pi/6$ (red dashed line), $\phi = \pi/4$ (black solid line), and $\phi = \pi/3$ (blue dash-dotted line), at three stages of the evolution: (a) $p = 0.25$, (b) $p = 0.5$, and (c) $p = 0.75$. In all cases the relative phase was fixed to its optimal value $\varphi = 0$. For each initial state and at fixed p, the channels that produce higher 3-tangle lead to higher maximal average fidelities. The nontrivial role of the initial entanglement $\mathcal{E}_0$ and the initial excited population $\mathcal{P}_1$ is observed (see the text for details).

If $\phi = \pi/4$ and $\varphi = 0$ then, at $p = 1$, the usual GHZ state $|\mathrm{GHZ}\rangle = \frac{1}{\sqrt{2}}(|000\rangle + |111\rangle)$ is reached, having null qubit-qubit entanglement and $\tau_{ABE_B} = 1$.

For $\zeta = 0$ the GC reduces to the AC and states that are equivalent (up to local unitary transformations) to W-type states arise. This can be seen by setting $\zeta = 0$ in Eq. (29), obtaining

$$\begin{aligned}|\psi_W\rangle &\equiv |\psi(\zeta = 0)\rangle \\ &= \cos\phi|000\rangle + e^{i\varphi}\sin\phi(\sqrt{1-p}|110\rangle \\ &\quad + \sqrt{p}|101\rangle). \end{aligned} \tag{42}$$

For $\phi = \arccos(1/\sqrt{3})$ and $\varphi = 0$ this state becomes, at $p = \frac{1}{2}$, equivalent (up to a local unitary transformation) to the usual W state $|W\rangle = \frac{1}{\sqrt{3}}(|000\rangle + |110\rangle + |101\rangle)$, characterized by having all qubit-qubit entanglements equal to $C_{ij} = \frac{2}{3}$ and a null 3-tangle.

Figure 7 depicts the evolution of $\mathbb{F}_{\max}$ for the initial states $|\psi_{\mathrm{GHZ}}\rangle|_{\phi=\pi/4,\varphi=0}$ (red solid line) and $|\psi_W\rangle|_{\phi=\arccos 1/\sqrt{3},\varphi=0}$ (blue dashed line). It shows that the maximal average fidelity improves when the resource state involves two qubits from a three-qubit system that evolves towards the state $|\mathrm{GHZ}\rangle$ rather than to $|W\rangle$.

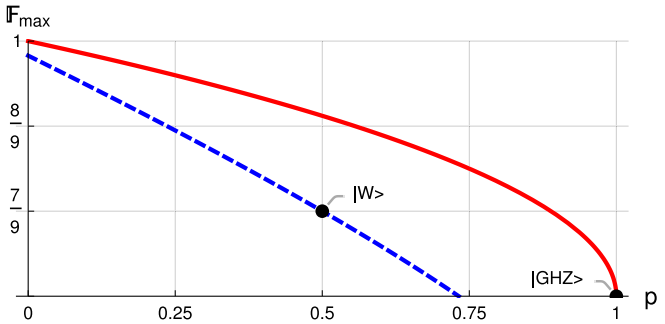

FIG. 7. Evolution of the maximal average fidelity (above the threshold value $\frac{2}{3}$), employing initial states that evolve towards the states $|\mathrm{GHZ}\rangle$ (red solid line) and $|W\rangle$ (blue dashed line), under the DC and the AC, respectively.

VI. FIDELITY AND FOUR-PARTITE ENTANGLEMENT GENERATED VIA NOISY CHANNELS

We now consider that both qubits A and B undergo local channels Λ_A and Λ_B, as a result of their separate interaction with initially uncorrelated qubits E_A and E_B. The initial resource state is thus [see Eqs. (1) and (11)]

$$|\psi_0\rangle = \cos\phi|0000\rangle + e^{i\varphi}\sin\phi|1100\rangle, \tag{43}$$

and the Kraus operators of the local channels are generically given by Eq. (12). Figure 8 shows the first two stages of the corresponding teleportation protocol.

Different forms of multipartite entanglement may arise in this four-qubit system [48]. Here we will focus on the multipartite entanglement as measured by the 4-tangle τ_4, defined for a four-qubit pure state $|\psi\rangle$ as [49]

$$\tau_4 = |\langle\psi|\sigma_y^{\otimes 4}|\psi^*\rangle|^2. \tag{44}$$

This quantity becomes maximal ($\tau_4 = 1$) for the four-partite GHZ state $\frac{1}{\sqrt{2}}(|0000\rangle + |1111\rangle)$ and vanishes for the four-partite W state $\frac{1}{\sqrt{4}}(|1000\rangle + |0100\rangle + |0010\rangle + |0001\rangle)$.

A. Two local generalized noisy channels

Assuming that Λ_A and Λ_B are generalized noisy channels, the corresponding Kraus operators read, following (27),

$$Q_0 = \begin{pmatrix} 1 & 0 \\ 0 & \sqrt{1-p_A} \end{pmatrix}, \quad Q_1 = \sqrt{p_A}\begin{pmatrix} 0 & \cos\zeta_A \\ 0 & \sin\zeta_A \end{pmatrix} \tag{45a}$$

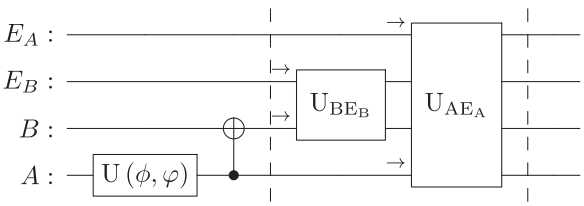

FIG. 8. Qubits A, B, E_A, and E_B are prepared in the state (43). The pairs A, E_A and B, E_B interact via unitary operations; thus A and B undergo local channels whose corresponding Kraus operators are $\{Q_\alpha\}$ and $\{K_\beta\}$.

and

$$K_0 = \begin{pmatrix} 1 & 0 \\ 0 & \sqrt{1-p_B} \end{pmatrix}, \quad K_1 = \sqrt{p_B}\begin{pmatrix} 0 & \cos\zeta_B \\ 0 & \sin\zeta_B \end{pmatrix}, \tag{45b}$$

with $\zeta_{A\,(B)} \in [0, \pi/2]$ the parameters that determine the specific channels and $0 \leqslant p_{A\,(B)} \leqslant 1$, again with $p_{A\,(B)}$ appropriate parametrizations of the evolution parameter of the transformation $U_{AE_A\,(BE_B)}$. Resorting to Eq. (13), the initial state (43) evolves into

$$\begin{aligned}|\psi\rangle_{ABE_AE_B} = (\cos\phi|00\rangle + e^{i\varphi}\sin\phi\sqrt{q_Aq_B}|11\rangle)|00\rangle + e^{i\varphi}\sin\phi[\sqrt{q_Ap_B}(\cos\zeta_B|10\rangle + \sin\zeta_B|11\rangle)|01\rangle \\ + \sqrt{p_Aq_B}(\cos\zeta_A|01\rangle + \sin\zeta_A|11\rangle)|10\rangle + \sqrt{p_Ap_B}(\cos\zeta_A|0\rangle + \sin\zeta_A|1\rangle)(\cos\zeta_B|0\rangle + \sin\zeta_B|1\rangle)|11\rangle],\end{aligned} \tag{46}$$

where $q_{A\,(B)} = 1 - p_{A\,(B)}$. From this state direct calculation gives

$$\begin{aligned}\tau_4 = p_Ap_B|\mathcal{E}_0\sin\zeta_A\sin\zeta_B \\ + 4e^{i\varphi}\mathcal{P}_1\sqrt{q_Aq_B}\cos\zeta_A\cos\zeta_B|^2.\end{aligned} \tag{47}$$

Unlike the previous case in which only B passes through the generalized channel, where C_{AB} was independent of the channel parameter ζ [see Eq. (30)], in the present scenario the entanglement of the resource state depends on both ζ_A and ζ_B. However, the general and explicit dependence of C_{AB} on ζ_A and ζ_B is far from trivial and will be omitted here. It suffices to recall that C_{AB} can be obtained from Eq. (19) using the resource state $\rho_{AB} = \mathrm{Tr}_{E_AE_B}|\psi\rangle\langle\psi|$, with $|\psi\rangle$ given by (46).

From Eq. (10) the maximal average fidelity for two GCs is $F_{\max} = \max_i\{F_{\Phi_i}\}$, with

$$F_{\Phi_i} = \frac{1}{3} + \frac{2}{3}\left\{\sum_{\alpha\beta}|\langle\Phi_i|Q_\alpha \otimes K_\beta|\phi_0\rangle|^2\right\}. \tag{48}$$

Substitution of the Kraus operators (45) gives

$$F_{\Phi^\pm} = \tfrac{2}{3} + \tfrac{1}{3}(\pm\mathcal{E}_0\sqrt{q_Aq_B}\cos\varphi - \mathcal{P}_1\Delta_\mp), \tag{49a}$$

$$F_{\Psi^\pm} = \tfrac{2}{3} - \tfrac{1}{3}(1 - \mathcal{P}_1\Delta_\pm), \tag{49b}$$

where $\Delta_\pm \in [0, 1]$ and is given by

$$\begin{aligned}\Delta_\pm = q_Bp_A\cos^2\zeta_A + q_Ap_B\cos^2\zeta_B \\ + p_Ap_B\sin^2(\zeta_A \pm \zeta_B).\end{aligned} \tag{50}$$

Consequently, $F_{\Psi^\pm} \leqslant \frac{2}{3}$; further, since $\zeta_A, \zeta_B \in [0, \pi/2]$, it holds that $\sin^2(\zeta_A + \zeta_B) \geqslant \sin^2(\zeta_A - \zeta_B)$, whence $\Delta_+ \geqslant \Delta_-$. This in turn leads us to

$$\cos\varphi \geqslant 0 \Rightarrow F_{\Phi^+} \geqslant F_{\Phi^-}, \tag{51}$$

so in the present case $\mathbb{F}_{\max}$, given by Eq. (6), is written as

$$\mathbb{F}^{\text{GC-GC}}_{\max\pm} = \tfrac{2}{3} + \tfrac{1}{3}\max\{0, [\mathcal{E}_0\sqrt{q_Aq_B}|\cos\varphi| - \mathcal{P}_1\Delta_\mp]\}, \tag{52}$$

where the upper (lower) sign must be chosen accordingly with

$$\cos\varphi \gtrless -\frac{1}{4}\frac{\sqrt{\mathcal{P}_1}}{\sqrt{1-\mathcal{P}_1}}\frac{1}{\sqrt{q_Aq_B}}(\Delta_+ - \Delta_-). \tag{53}$$

As follows from (52), the optimal phase φ is the same as in the previous cases, namely, $\varphi = 0, \pi$. Also, a loss in the fidelity emerges, encoded in the negative term proportional to $\mathcal{P}_1$.

B. Fidelity and multipartite entanglement for four qubits under parallel generalized noisy channels

In our forthcoming analysis, we will simplify the equations taking $p_A = p_B = p$.[3] Equation (47) thus reads

$$\begin{aligned}\tau_4 = p^2[\mathcal{E}_0\sin\zeta_A\sin\zeta_B + 4\mathcal{P}_1(1-p)\cos\zeta_A\cos\zeta_B]^2 \\ - 2\mathcal{E}_0\mathcal{P}_1p^2(1-p)\sin 2\zeta_A\sin 2\zeta_B(1-\cos\varphi).\end{aligned} \tag{54}$$

Recalling that $\zeta_{A,B} \in [0, \pi/2]$, the second line in Eq. (54) is a nonpositive term that reduces the amount of four-partite entanglement. Notice, however, that for $\varphi = 0$ such a term vanishes, and consequently the relative phase that maximizes τ_4 maximizes also $\mathbb{F}^{\text{GC-GC}}_{\max\pm}$. By choosing this optimal phase, Eq. (53) holds with the upper inequality sign and accordingly Eq. (52) reduces to

$$\begin{aligned}\mathbb{F}^{\text{GC-GC}}_{\max} = \tfrac{2}{3} + \tfrac{1}{3}\max\{0, [\mathcal{E}_0(1-p) - \mathcal{P}_1p[p\sin^2(\zeta_A - \zeta_B) \\ + (1-p)(\cos^2\zeta_A + \cos^2\zeta_B)]]\},\end{aligned} \tag{55}$$

whereas τ_4 becomes

$$\tau_4 = [\mathcal{E}_0p\sin\zeta_A\sin\zeta_B + 4\mathcal{P}_1p(1-p)\cos\zeta_A\cos\zeta_B]^2. \tag{56}$$

If $\mathcal{E}_0p \geqslant 4\mathcal{P}_1p(1-p)$ then

$$\mathcal{E}_0p\cos\zeta_A\cos\zeta_B \geqslant 4\mathcal{P}_1p(1-p)\cos\zeta_A\cos\zeta_B, \tag{57}$$

whence, by adding $\mathcal{E}_0p\sin\zeta_A\sin\zeta_B$ on both sides of the inequality, we get

$$\mathcal{E}_0p\cos(\zeta_A - \zeta_B) \geqslant \sqrt{\tau_4}. \tag{58}$$

An analogous reasoning applies for $\mathcal{E}_0p \leqslant 4\mathcal{P}_1p(1-p)$, so we finally get

$$\tau_4 \leqslant T^2\cos^2(\zeta_A - \zeta_B), \tag{59}$$

where $T = \max\{\mathcal{E}_0p, 4\mathcal{P}_1p(1-p)\}$. This means that the maximum value of τ_4 over all possible channels is located along the line $\zeta_A = \zeta_B = \zeta$ and explicitly reads

$$\tau_4^{\max} = \begin{cases}\mathcal{E}_0^2p^2 = \tau_4|_{\zeta=\pi/2} & \text{if } \mathcal{E}_0 \geqslant 4\mathcal{P}_1(1-p) \\ 16\mathcal{P}_1^2p^2(1-p)^2 = \tau_4|_{\zeta=0} & \text{if } \mathcal{E}_0 \leqslant 4\mathcal{P}_1(1-p).\end{cases} \tag{60}$$

The maximum four-partite entanglement is thus reached whenever both channels are either DC or AC. In the former

[3]This means that the evolution parameters of U_{AE_A} and U_{BE_B} are the same (for example, they are both the time t) and the parametrizations are identical, so $p(t)$ is the same for both pairs of Kraus operators (45).

case also $\mathbb{F}_{\max}^{\text{GC-GC}}$ reaches its maximum value, over all GC-GC combinations. This can be seen by noticing that the loss in the fidelity, encoded in the (nonpositive) term proportional to $\mathcal{P}_1 p$ in Eq. (55), vanishes irrespective of the initial state and the evolution parameter only for $\zeta_A = \zeta_B = \pi/2$, resulting in

$$\begin{aligned}\mathbb{F}_{\max}^{\text{GC-GC}} \leqslant \mathbb{F}_{\max}^{\text{DC-DC}} &= \tfrac{2}{3} + \tfrac{1}{3}\mathcal{E}_0(1-p) \\ &= \tfrac{2}{3} + \tfrac{1}{3}C_{AB}^{\text{DC-DC}}(p),\end{aligned} \tag{61}$$

where $C_{AB}^{\text{DC-DC}} = \mathcal{E}_0(1-p)$ stands for the entanglement of the resource state when two parallel DCs are implemented. Consequently, whenever the condition in the first line of (60) holds, i.e., whenever

$$1 - \frac{1}{2}\sqrt{\frac{1-\mathcal{P}_1}{\mathcal{P}_1}} \leqslant p, \tag{62}$$

the channel that maximizes τ_4 maximizes also $\mathbb{F}_{\max}^{\text{GC-GC}}$. Note that (62) is satisfied for all p provided $\mathcal{P}_1 \leqslant \frac{1}{5}$, that is, for sufficiently low populations $\mathcal{P}_1$, the maximal value of τ_4 and of $\mathbb{F}_{\max}^{\text{GC-GC}}$ are jointly reached.

If the condition (62) is not met, $\tau_4^{\max}$ is given by the second line in Eq. (60) and corresponds to $\zeta_A = \zeta_B = 0$, i.e., to the AC-AC combination. In this case (55) reduces to

$$\begin{aligned}\mathbb{F}_{\max}^{\text{AC-AC}} &= \tfrac{2}{3} + \tfrac{1}{3}C_{AB}^{\text{AC-AC}}(p) \\ &= \max\left\{\tfrac{2}{3}, \mathbb{F}_{\max}^{\text{DC-DC}} - \tfrac{2}{3}\mathcal{P}_1 p(1-p)\right\},\end{aligned} \tag{63}$$

where in the first line we used that, under parallel ACs, $C_{AB}^{\text{AC-AC}} = \max\{0, (1-p)(\mathcal{E}_0 - 2\mathcal{P}_1 p)\}$.

Now, from Eq. (55) we obtain the expression for $\mathbb{F}_{\max}^{\text{GC-GC}}$ along the line $\zeta_A = \zeta_B = \zeta$,

$$\begin{aligned}\mathbb{F}_{\max}^{\text{GC-GC}}(\zeta) = \tfrac{2}{3} + \tfrac{1}{3}\max\{0, [&\mathcal{E}_0(1-p) \\ &- 2\mathcal{P}_1 p(1-p)\cos^2\zeta]\},\end{aligned} \tag{64}$$

whose minimum above the threshold value $\frac{2}{3}$ corresponds to the AC-AC combination. This observation, together with the fact that $\tau_4^{\max}$ is attained at $\zeta_A = \zeta_B = \zeta = 0, \pi/2$, indicates that the channels that maximize the four-partite entanglement are not always those that maximize $\mathbb{F}_{\max}^{\text{GC-GC}}$. Rather, $\mathbb{F}_{\max}^{\text{GC-GC}}$ is either maximal or minimal (within the family of twin channels with $\zeta_A = \zeta_B = \zeta$) on points where the 4-tangle is maximal.

As for the vanishing value of τ_4, we see from Eq. (56) that it corresponds to the combination of a DC on either one of the qubits and an AC on the other one. This null 4-tangle is accompanied by the maximal average fidelity

$$\begin{aligned}\mathbb{F}_{\max}^{\text{AC-DC}} = \mathbb{F}_{\max}^{\text{DC-AC}} &= \tfrac{2}{3} + \tfrac{1}{3}\max\{0, \mathcal{E}_0(1-p) - \mathcal{P}_1 p\} \\ &= \max\left\{\tfrac{2}{3}, \mathbb{F}_{\max}^{\text{DC-DC}} - \tfrac{1}{3}\mathcal{P}_1 p\right\},\end{aligned} \tag{65}$$

an expression that is analogous to Eq. (40) for the case with a vanishing 3-tangle (AC).

In order to make a complete analysis of the relation between τ_4 and $\mathbb{F}_{\max}^{\text{GC-GC}}$, a key element should be considered, namely, the entanglement of the resource state. The evolution of C_{AB} and $\mathbb{F}_{\max}^{\text{GC-GC}}$ for a given initial state and fixed channel parameters is qualitatively similar to that shown in Fig. 5, i.e., the quantum channel induces a loss in C_{AB}, which is verified by noticing that Eq. (55) is a decreasing function of p. Yet, as occurred in the tripartite case, there exists a positive correlation between $\mathbb{F}_{\max}^{\text{GC-GC}}$ and the multipartite entanglement (here measured by τ_4) that holds at each stage of the evolution and for a fixed amount of C_{AB}. In order to verify this, it becomes crucial to recall first an important difference between the three- and the four-partite scenarios: As mentioned below Eq. (47), in the former case C_{AB} is independent of ζ (hence is the same for all channels), whereas in the four-qubit example C_{AB} typically varies with both channel parameters ζ_A and ζ_B. This observation, together with the essential role played by the entanglement of the resource state in the teleportation success, calls for an analysis that incorporates the value of C_{AB} when examining the dynamic interplay between τ_4 and $\mathbb{F}_{\max}^{\text{GC-GC}}$. To this end, we compare the effect of various channels (scanned by varying ζ_A and ζ_B) on the quantities of interest, namely τ_4, $\mathbb{F}_{\max}^{\text{GC-GC}}$, and C_{AB}, at the same stage of the evolution for different initial states. We do so by constructing triads $(\tau_4, \mathbb{F}_{\max}^{\text{GC-GC}}, C_{AB})$, which for a given p and fixed initial parameters φ and ϕ depend only on ζ_A and ζ_B. We then consider 16 384 different channels (pairs $\{\zeta_A, \zeta_B\}$) and display the resulting triads as points in the plane $(\tau_4, \mathbb{F}_{\max}^{\text{GC-GC}})$ colored according to the corresponding range of values of C_{AB}. Figure 9 shows the ensuing triads for $\varphi = 0$ and different values of ϕ (rows) and p (columns). In all cases, τ_4 and $\mathbb{F}_{\max}^{\text{GC-GC}}$ were directly computed from Eqs. (56) and (55), respectively, whereas C_{AB} was numerically calculated as explained below Eq. (47).

All points in each panel of Fig. 9 lie within a region delimited by three curves: the black solid line, encompassing the family of twin channels with $\zeta_A = \zeta_B = \zeta$; the blue dashed line, including those cases where one of the qubits (either A or B) undergoes an AC, meaning $\zeta_{A\,(B)} = 0$, while the other one undergoes an arbitrary GC; and the red dash-dotted line, comprising the channels where one of the qubits (either A or B) undergoes a DC, so $\zeta_{A\,(B)} = \pi/2$, while the other one is subject to an arbitrary GC. Accordingly, the vertices of the regions are identified as follows: Blue triangles represent the AC-DC (or DC-AC) combination, with $\tau_4 = 0$ and the maximal average fidelity given by (65); red stars correspond to the DC-DC combination, where $\mathbb{F}_{\max}^{\text{GC-GC}}$ reaches its maximum value, in line with Eq. (61); and black circles represent the AC-AC combination and correspond to points with the lowest $\mathbb{F}_{\max}^{\text{GC-GC}}$ along the line of twin channels, in agreement with the statement below Eq. (64).

In all the graphs in Fig. 9, the colored bands, containing points whose C_{AB} lies within a specific range of values, reveal a positive correlation between the 4-tangle and the maximal average fidelity. Such correlation persists as the width of the range is reduced, as exemplified in Table II showing values of C_{AB}, τ_4, and $\mathbb{F}_{\max}^{\text{GC-GC}}$ taken from Fig. 9(e). The values of τ_4 and $\mathbb{F}_{\max}^{\text{GC-GC}}$ are displayed in increasing order and both increase simultaneously as the value of C_{AB} (numerically obtained) remains constant (up to four digits). The results indicate that despite the specificities present in each panel of Fig. 9, a feature common to all of them is that for a fixed entanglement of the resource state C_{AB}, $\mathbb{F}_{\max}^{\text{GC-GC}}$ increases as τ_4 increases.

In other words, for a given initial state (ϕ fixed), at each stage of the evolution (p fixed), from among all the GC-GC combinations that correspond to the same entanglement of the resource state, those that generate higher amounts of four-partite entanglement lead to higher fidelities. This conclusion

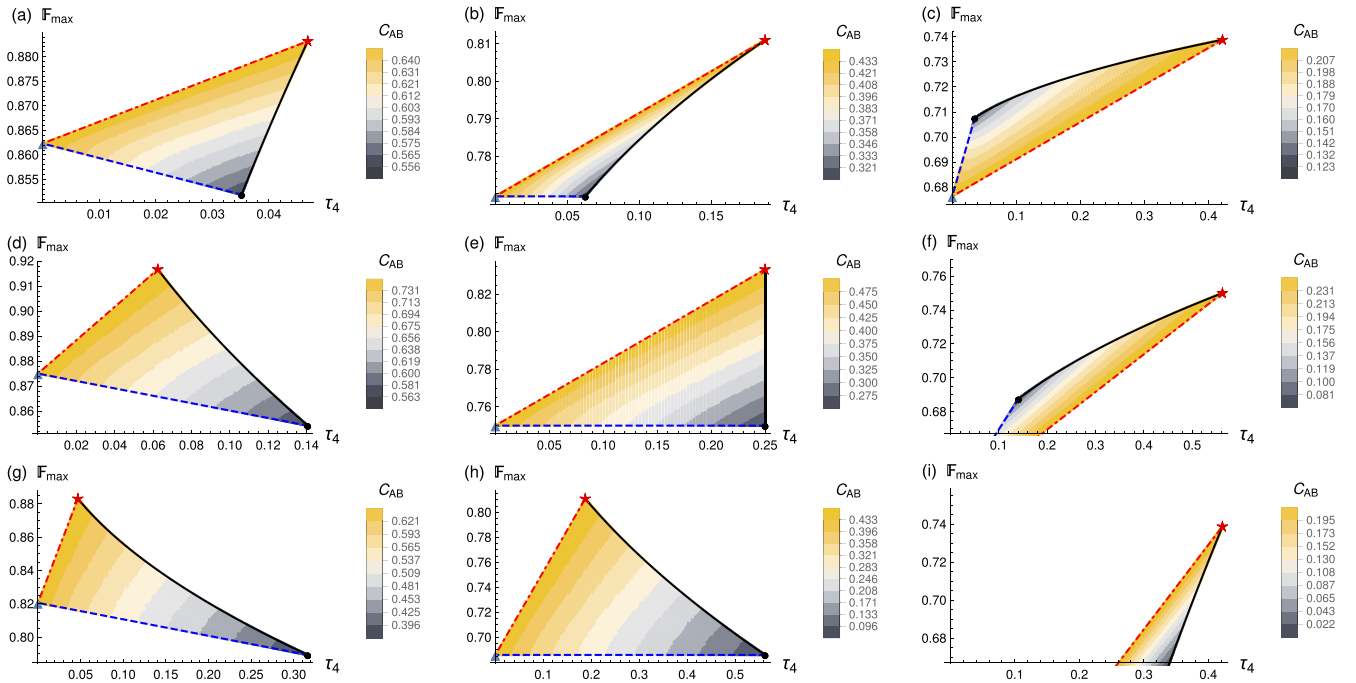

FIG. 9. Plot of $\mathbb{F}_{\max}^{\text{GC-GC}}$ versus τ_4 for (a)–(c) $\phi = \pi/6$, (d)–(f) $\phi = \pi/4$, and (g)–(i) $\phi = \pi/3$ and (a), (d), and (g) $p = 0.25$; (b), (e), and (h) $p = 0.5$; and (c), (f), and (i) $p = 0.75$. The regions are generated as all the channels are considered (by varying ζ_A and ζ_B), and the color scale indicates the amount of entanglement of the corresponding resource state C_{AB}. The confining curves comprise different families of channels: twin channels with $\zeta_A = \zeta_B = \zeta$ along the black solid curve, an AC-GC (or a GC-AC) combination along the blue dashed curve, and a DC-GC (or a GC-DC) combination along the red dash-dotted curve. Black circles correspond therefore to $\zeta_A = \zeta_B = 0$ (parallel ACs), red stars to $\zeta_A = \zeta_B = \pi/2$ (parallel DCs), and blue triangles to a combination of $\zeta_{A\,(B)} = 0$ and $\zeta_{B\,(A)} = \pi/2$ (AC-DC and DC-AC hybrids).

is analogous to that reached in the three-partite case, indicating that the multipartite entanglement may act as a resource that protects the teleportation fidelity against the noisy channel (provided the same amount of C_{AB} is available).

For the values of ϕ and p considered in Figs. 9(a)–9(c), 9(f), and 9(i), the condition (62) is satisfied and accordingly the maximum of $\mathbb{F}_{\max}^{\text{GC-GC}}$ is reached along with the maximum of the 4-tangle, given in this case by $\tau_4^{\max} = \mathcal{E}_0^2 p^2$. In contrast, the cases depicted in Figs. 9(d), 9(g), and 9(h) do not comply with the inequality (62) and thus correspond to $\tau_4^{\max} = 16\mathcal{P}_1^2 p^2 (1-p)^2$ and $\mathbb{F}_{\max}^{\text{GC-GC}} = \mathbb{F}_{\max}^{\text{AC-AC}}$, that is, to the minimal fidelity along the black solid curve. Figure 9(e) corresponds to the case in which $\mathcal{E}_0 = 4\mathcal{P}_1(1-p)$, so as follows from Eq. (60) the maximum value of τ_4 is attained simultaneously at the red star (DC-DC) and the black circle (AC-AC).

In all panels of Fig. 9 it is observed that as the black solid curve is traversed from the black circle to the red star, C_{AB} increases along with $\mathbb{F}_{\max}^{\text{GC-GC}}$, so the highest fidelity is reached along with the highest C_{AB}. This shows that, within the family of twin channels, the resource state's entanglement helps to improve the maximal average fidelity. However, this does not hold for other channels. For example, as the blue dashed line is traversed from the black circle to the blue triangle, that is, along the family of AC-GC combinations, there are cases in which an increase in C_{AB} is accompanied by a decrease in $\mathbb{F}_{\max}^{\text{AC-GC}}$, like the one depicted in Fig. 9(c). In such case it is only the 4-tangle that is seemingly enhancing the maximal average fidelity. Further, for the family of DC-GC combinations, as the red dash-dotted line is traversed, C_{AB} is kept constant (for fixed p) and maximal [in fact, in this case we get $C_{AB}^{\text{DC-GC}} = \mathcal{E}_0(1-p)$] and the improvement of $\mathbb{F}_{\max}^{\text{DC-GC}}$ is therefore ascribable to the increase of τ_4.

TABLE II. Values of C_{AB}, τ_4, and $\mathbb{F}_{\max}^{\text{GC-GC}}$ extracted from Fig. 9(e) (corresponding to $\phi = \pi/4$, $\varphi = 0$, and $p = 0.5$), for different values of the channels parameters ζ_A and ζ_B.

ζ_A/π	ζ_B/π	C_{AB}	τ_4	$\mathbb{F}_{\max}^{\text{GC-GC}}$
181/500	37/500	0.422003	0.0954376	0.760765
91/250	2/25	0.422002	0.0984991	0.761839
93/250	29/250	0.422003	0.120289	0.768959
187/500	143/1000	0.422001	0.139887	0.774978
187/500	19/125	0.422008	0.146878	0.777085
369/1000	99/500	0.422009	0.18453	0.788234
42/125	281/1000	0.422005	0.24261	0.805185
167/500	71/250	0.422008	0.243882	0.805556

VII. CONCLUSION

We investigated the role of multipartite entanglement in the dynamics of the maximal average fidelity (above the classical threshold value) when the teleportation protocol includes the action of a local quantum channel $\Lambda_{AB} = \Lambda_A \otimes \Lambda_B$, acting on the qubits A and B that comprise the resource state. To facilitate our goal, we expressed the maximal average fidelity in terms of the Kraus operators corresponding to

a general two-qubit channel [Eq. (8)] and introduced the Kraus operators of a generalized noisy channel [Eq. (27)], which encompasses the paradigmatic amplitude damping and dephasing channels and connects them via a continuous parameter that also determines the amount of multipartite entanglement created along the evolution.

We first considered the case $\Lambda_A = \mathrm{I}_2$, with Λ_B representing the generalized noisy channel, rooted at the interaction of B with an additional qubit E_B. Three-partite entanglement thus typically emerges among the qubits A, B, and E_B, here quantified by the 3-tangle τ_{ABE_B}. In the second scenario, both Λ_A and Λ_B correspond to generalized channels. Interpreting them as the effective result of a local interaction of A and B with additional qubits E_A and E_B, we focused on the ensuing four-partite entanglement among the parties A, B, E_A, and E_B, as measured by τ_4.

In both cases, we found that the relative phase φ that optimizes both $\mathbb{F}_{\max}$ and τ_4 is $\varphi = 0$. More importantly, the analytical and numerical analysis (considering identically parametrized channels in the four-party case) revealed that for a fixed nonzero amount of the resource state's entanglement (i.e., for fixed $C_{AB} \neq 0$), at each stage of the evolution, the teleportation success improves under channels that induce higher amounts of multipartite entanglement. Here it is important to stress that both the 3-tangle and the 4-tangle quantify a specific type of multipartite entanglement, namely, the three-way and the four-way entanglement, respectively, characteristic of GHZ-type states, and thereby absent in W-type states [42,49]. Consequently, our findings indicate that it is specifically the amount of GHZ-type entanglement which favors better teleportation fidelities. It should be stressed that this conclusion does not go against the (expected) fact that, given a specific noisy channel (a fixed ζ), as the evolution takes place the teleportation fidelity decays while the 3- and 4-tangles may increase; rather, the conclusion compares the effect of different generalized noisy channels on $\mathbb{F}_{\max}$ throughout the evolution and establishes that under channels that produce more multipartite (GHZ-type) entanglement, the detrimental effects on $\mathbb{F}_{\max}$ are lessened. Further, when C_{AB} vanishes, as occurs at $p = 1$, when the channel has suppressed all the entanglement of the resource state, the maximal average fidelity drops below the classical threshold value, despite that the multipartite entanglement may acquire relatively large values. This highlights C_{AB} as a necessary element that triggers the power of the n-way entanglement to enhance the teleportation success.

In the three-party case, C_{AB} is the same for all the channels considered, and the relation between $\mathbb{F}_{\max}^{\mathrm{GC}}$ and τ_{ABE_B} was clearly revealed, along with the identification of the DC as the channel that produces the higher values of $\mathbb{F}_{\max}^{\mathrm{GC}}$. In the four-qubit case, in contrast, C_{AB} depends on the specific channel and the relation between $\mathbb{F}_{\max}^{\text{GC-GC}}$ and τ_4 only (i.e., without considering the value of C_{AB}) is more subtle than in the three-party counterpart. In particular, we found that an increment in τ_4 induces an increment in $\mathbb{F}_{\max}^{\text{GC-GC}}$, irrespective of the initial state and stage of the evolution, only when the composite channel is the DC-GC combination, that is, when either one of the qubits is subject to a dephasing channel. Notably, in this case, C_{AB} does not depend on the specific GC and the enhancement of the maximal average fidelity is due solely to the increase in the four-partite entanglement.

For the families of twin GC-GC with $\zeta_A = \zeta_B = \zeta$ and AC-GC, a higher value of τ_4 is not always accompanied by a higher value of $\mathbb{F}_{\max}^{\text{GC-GC}}$, ultimately because C_{AB} changes with the channels' parameters. Instead, for a fixed initial state and at a given stage of the evolution, the composite channel for which the 4-tangle is maximal is either DC-DC, in which case $\mathbb{F}_{\max}^{\text{GC-GC}}$ attains its global maximal value, or AC-AC, corresponding to an $\mathbb{F}_{\max}^{\text{GC-GC}}$ that is minimal within the family of twin channels ($\zeta_A = \zeta_B = \zeta$).

Interestingly, guaranteeing that $\mathbb{F}_{\max}$ exceeds the classically attainable value depends not only on the initial entanglement at disposal, but also on the initial population $\mathcal{P}_1$ of the state $|11\rangle_{AB}$, which plays against the improvement of the teleportation success. Further, for sufficiently low values of $\mathcal{P}_1$ ($\mathcal{P}_1 \leqslant 0.2$), the maximal value of τ_4 is attained together with the maximal value of $\mathbb{F}_{\max}^{\text{GC-GC}}$.

Our analysis led us to conclude that the previously reported improvement of the teleportation fidelity under some types of noisy channels [10–15] may be rooted in the emergence of multipartite entanglement induced by the interaction of the resource qubits with their surroundings. This offers valuable insights into the power of multipartite correlations as well as into the characterization of the processes that better protect the teleportation fidelity in the more realistic scenario in which $A + B$ is an open system. In particular, processes that generate GHZ-type states in the three- or four-qubit system have the potential to assist the protocol by reducing the detrimental effects of noise, as a result of the induced generation of three- and four-way entanglement. This highlights the GHZ-type entanglement as a useful auxiliary resource in noisy quantum teleportation.

ACKNOWLEDGMENTS

The authors acknowledge financial support from DGAPA, UNAM through Project No. PAPIIT IN112723. V.H.T.B. acknowledges CONAHCYT scholarship with CVU No. 863195.

[1] C. H. Bennett, G. Brassard, C. Crépeau, R. Jozsa, A. Peres, and W. K. Wootters, Phys. Rev. Lett. **70**, 1895 (1993).
[2] K. Banaszek, Phys. Rev. Lett. **86**, 1366 (2001).
[3] S. Popescu, Phys. Rev. Lett. **72**, 797 (1994).
[4] R. Horodecki, M. Horodecki, and P. Horodecki, Phys. Lett. A **222**, 21 (1996).
[5] D. Bussandri, M. Portesi, and A. Majtey, Physica A **592**, 126853 (2022).
[6] S. Oh, S. Lee, and H.-w. Lee, Phys. Rev. A **66**, 022316 (2002).
[7] L.-N. Jiang, Int. J. Theor. Phys. **58**, 3899 (2019).
[8] S. Harraz, S. Cong, and J. J. Nieto, EPJ Quantum Technol. **9**, 15 (2022).

[9] D.-G. Im, C.-H. Lee, Y. Kim, H. Nha, M. S. Kim, S.-W. Lee, and Y.-H. Kim, npj Quantum Inf. **7**, 86 (2021).
[10] P. Badziag, M. Horodecki, P. Horodecki, and R. Horodecki, Phys. Rev. A **62**, 012311 (2000).
[11] S. Bandyopadhyay, Phys. Rev. A **65**, 022302 (2002).
[12] R. Fortes and G. Rigolin, Phys. Rev. A **92**, 012338 (2015).
[13] S. Ahadpour and F. Mirmasoudi, Rev. Mex. Fís. **66**, 378 (2020).
[14] A. Fonseca, Phys. Rev. A **100**, 062311 (2019).
[15] L. T. Knoll, C. T. Schmiegelow, and M. A. Larotonda, Phys. Rev. A **90**, 042332 (2014).
[16] J. Lee, H. Min, and S. D. Oh, Phys. Rev. A **66**, 052318 (2002).
[17] V. Gorbachev, A. Trubilko, A. Rodichkina, and A. Zhiliba, Phys. Lett. A **314**, 267 (2003).
[18] Y. Yeo and W. K. Chua, Phys. Rev. Lett. **96**, 060502 (2006).
[19] Z.-X. Man, Y.-J. Xia, and N. B. An, Phys. Rev. A **75**, 052306 (2007).
[20] G. Rigolin, Phys. Rev. A **71**, 032303 (2005).
[21] W. Li, X.-W. Zha, and J.-X. Qi, Int. J. Theor. Phys. **55**, 3927 (2016).
[22] B. S. Choudhury and A. Dhara, Int. J. Theor. Phys. **57**, 1 (2018).
[23] M. Wang and H.-S. Li, Quantum Inf. Process. **21**, 44 (2022).
[24] N. Singh, N. Singh, A. Pathak, V. Verma, and R. S. Singh, Opt. Quantum Electron. **55**, 932 (2023).
[25] E. Jung, M.-R. Hwang, Y. H. Ju, M.-S. Kim, S.-K. Yoo, H. Kim, D. K. Park, J.-W. Son, S. Tamaryan, and S.-K. Cha, Phys. Rev. A **78**, 012312 (2008).
[26] G. Yang, B.-W. Lian, M. Nie, and J. Jin, Chin. Phys. B **26**, 040305 (2017).
[27] X.-P. Han and J.-M. Liu, Phys. Scr. **78**, 015001 (2008).
[28] H. Xiao-Ping and L. Jin-Ming, Commun. Theor. Phys. **49**, 895 (2008).
[29] S. Ishizaka, Phys. Rev. A **63**, 034301 (2001).
[30] N. Van Hop, Quantum Inf. Process. **18**, 340 (2019).
[31] L. Ruan, W. Dai, and M. Z. Win, Phys. Rev. A **97**, 052332 (2018).
[32] H. Weinfurter, Europhys. Lett. **25**, 559 (1994).
[33] S. L. Braunstein and A. Mann, Phys. Rev. A **51**, R1727 (1995).
[34] G. D'Ariano, P. Lo Presti, and M. Sacchi, Phys. Lett. A **272**, 32 (2000).
[35] P. Agrawal and A. K. Pati, Phys. Lett. A **305**, 12 (2002).
[36] M. Horodecki, P. Horodecki, and R. Horodecki, Phys. Rev. A **60**, 1888 (1999).
[37] C. H. Bennett, D. P. DiVincenzo, J. A. Smolin, and W. K. Wootters, Phys. Rev. A **54**, 3824 (1996).
[38] S. Massar and S. Popescu, Phys. Rev. Lett. **74**, 1259 (1995).
[39] K. Kraus, Ann. Phys. (NY) **64**, 311 (1971).
[40] W. K. Wootters, Phys. Rev. Lett. **80**, 2245 (1998).
[41] A. Valdés-Hernández, V. H. T. Brauer, and F. S. Zamora, Eur. Phys. J. D **73**, 245 (2019).
[42] W. Dür, G. Vidal, and J. I. Cirac, Phys. Rev. A **62**, 062314 (2000).
[43] V. Coffman, J. Kundu, and W. K. Wootters, Phys. Rev. A **61**, 052306 (2000).
[44] P. Rungta, V. Bužek, C. M. Caves, M. Hillery, and G. J. Milburn, Phys. Rev. A **64**, 042315 (2001).
[45] L. Aolita, F. de Melo, and L. Davidovich, Rep. Prog. Phys. **78**, 042001 (2015).
[46] O. J. Farías, G. H. Aguilar, A. Valdés-Hernández, P. H. Souto Ribeiro, L. Davidovich, and S. P. Walborn, Phys. Rev. Lett. **109**, 150403 (2012).
[47] G. H. Aguilar, O. J. Farías, A. Valdés-Hernández, P. H. Souto Ribeiro, L. Davidovich, and S. P. Walborn, Phys. Rev. A **89**, 022339 (2014).
[48] G. H. Aguilar, A. Valdés-Hernández, L. Davidovich, S. P. Walborn, and P. H. Souto Ribeiro, Phys. Rev. Lett. **113**, 240501 (2014).
[49] A. Wong and N. Christensen, Phys. Rev. A **63**, 044301 (2001).